A model predictive control approach towards the energy efficiency of submerged dredging

Bakker, Mathijs; Coraddu, Andrea; Hijdra, Rolph

DOI
10.1016/j.oceaneng.2023.115770

Publication date
2023

Document Version
Final published version

Published in
Ocean Engineering

Ocean Engineering 287 (2023) 115770

Contents lists available at ScienceDirect

Ocean Engineering

journal homepage: www.elsevier.com/locate/oceaneng

A model predictive control approach towards the energy efficiency of submerged dredging

Mathijs Bakker [b], Andrea Coraddu [a,*], Rolph Hijdra [b]

[a] Delft University of Technology, The Netherlands
[b] C-Job Naval Architects, Capelle aan den IJsel, The Netherlands

ARTICLE INFO

Keywords:
Underwater vehicles
Model predictive control
Dredging
Monte Carlo simulation
Autonomous shipping

ABSTRACT

Autonomous submerged dredging offers numerous benefits, such as reduced ship resistance and lower vacuum requirements for the dredge pumps. However, this method also presents new challenges, such as stability and buoyancy control, which must be addressed to minimize the energy requirements and ensure cost-effectiveness and sustainability. To achieve these goals, this paper proposes a Model Predictive Control (MPC) strategy to minimize control effort and energy requirements. Compared to traditional motion control methods such as proportional–integral–derivative (PID) control, MPC shows great promise in terms of energy efficiency and trajectory-tracking. The Autonomous Low Energy Replenishment Dredger (ALERD) is used as a case study to showcase the potential of the proposed control strategy. A time-domain simulation model is developed, and the ALERD is modeled as an underwater vehicle using a state-space representation. The classic PID control and the proposed MPC framework are compared in terms of trajectory-tracking, energy requirements, and robustness to modeling uncertainties, using sensitivity analysis. The results show that the proposed MPC control framework outperforms PID control in all aspects considered. Furthermore, a comparison between the energy requirements of the ALERD and a conventional dredger, for the same operational profile and hopper volume, indicates that autonomous submerged dredging can potentially decrease total energy requirements by 66%.

1. Introduction

The Autonomous Low Energy Replenishment Dredger (ALERD) is a unique underwater vehicle intended for submerged dredging along the Dutch Coastline to perform coastal replenishment, developed during the Innovations in the Coastline Care program of the Dutch General Directorate for Public Works and Water Management (Rijkswaterstaat). Rijkswaterstaat has the ambition to decrease their emissions to zero at the latest by 2030 and is therefore looking at sustainable and cost-effective solutions for coastal maintenance along the Dutch coast. For the ALERD to be cost-effective even with an expensive zero-emission energy supply, the total energy consumption should be minimized to reduce the systems needed for delivering this energy, which reduces the cost-price making it a cost-effective solution. In fact, as reported in Hijdra and Van Der Harst (2019), the power for propulsion can be reduced by 55% due to the absence of wave-making and breaking resistance, and the required power for the dredging pumps can be reduced by 80% due to the decreased suction depth. For underwater vehicles, the stability and buoyancy must be actively controlled, which requires an additional amount of energy compared to conventional ships (Renilson, 2015). This energy requirement should be minimized to achieve cost-effective solutions and show the benefits of autonomous submerged dredging compared to conventional dredging.

Conventional remotely operated vehicles or autonomous underwater vehicles are controlled through several key variables (Jordán and Bustamante, 2009). These typically include: (i) Depth/Altitude, controlled by adjusting the vehicle's buoyancy or using vertical thrusters; (ii) Speed, controlled by varying the thrust provided by the vehicle's propulsion system; (iii) Heading/Yaw, usually controlled by the rudder in surface vehicles, or by differential or vector thrust in fully submerged vehicles; (iv) Pitch and Roll, controlled by redistributing weight, adjusting buoyancy in different sections of the vehicle, or through the use of control surfaces or thrusters; (v) Position, often controlled indirectly through a combination of speed, heading, and depth controls, and may use GPS or acoustic positioning systems when near the surface, and inertial or Doppler navigation systems when submerged; (vi) Buoyancy Control, affecting the vehicle's depth and trim by regulating the volume of the ballast tanks or the power of buoyancy control devices.

For controlling underwater vehicles, Proportional–Integral–Derivative (PID) control is widely used in underwater vehicle control due to the ease of practical implementation (Long et al., 2021; Sahoo

* Corresponding author.
E-mail addresses: ma.bakker@c-job.com (M. Bakker), a.coraddu@tudelft.nl (A. Coraddu), r.hijdra@c-job.com (R. Hijdra).

https://doi.org/10.1016/j.oceaneng.2023.115770
Received 17 May 2023; Received in revised form 22 August 2023; Accepted 3 September 2023
Available online 11 September 2023

et al., 2019). PID is often used for flight control, namely controlling small autonomous underwater vehicles' combined depth and pitch motion (AUVs) (Jalving, 1994; Yildiz et al., 2009; Steenson et al., 2011; Tanakitkorn et al., 2017; Carrica et al., 2019). According to Zhang et al. (2019), PID control strategies are often considered less accurate for trajectory tracking and path following and unsuitable for nonlinear models and uncertain external disturbances. Moreover, it also needs careful tuning, which can be done manually, or by using tuning rules or tuning algorithms. To overcome these limitations and increase PID control's performance, adaptive tuning algorithms for PID controllers are developed (Sahoo et al., 2019; Rout and Subudhi, 2017; Kong et al., 2020; Xiang et al., 2017). Most advanced control strategies proposed in the literature focus on controlling small AUVs, designing motion control methods for trajectory-tracking and path-following, and taking care of the unknown dynamics, system non-linearity, and unknown disturbances (Londhe and Patre, 2019). Authors of Ma et al. (2021) focused on modeling and controlling a subsea shuttle tanker, which is one of the first studies considering a large underwater vehicle. The authors concluded that classical PID control is insufficient for controlling the depth of large underwater vehicles, such as the subsea shuttle tanker, and a feed-forward control strategy is proposed, such as MPC.

In the literature, more advanced methods of motion control for trajectory-tracking and path-following are described, such as Backstepping Control (BSC), Fuzzy Logic Control (FLC), Neural Network Control (NNC), Robust Adaptive Control (RAC), Sliding Mode Control (SMC), and Model Predictive Control (MPC). These motion control methods are used to address the complex dynamic control problem associated with AUVs (Sahoo et al., 2019).

Authors of Yan et al. (2020) used BSC in combination with the Lyapunov direct method for controlling a multi-input multi-output system such as underwater vehicles. Nonetheless, authors of Yan et al. (2020) reported that BSC cannot solve the uncertainty of system parameters and external disturbances and is, therefore, less applicable for underwater vehicles. Moreover, according to Zhang et al. (2019), the computing complexity increases rapidly as the system order increases because of the repeated differentiation of virtual controllers.

Authors of Kong et al. (2020) applied FLC to effectively control an underwater vehicle. Their approach is not dependent on an accurate mathematical model and, therefore can easily be used to control uncertain and strong nonlinear systems. Authors of Xiang et al. (2017) reported that for inaccurate model parameters, the fuzzy PID controller has a better performance compared to a traditional PID controller. Furthermore, the fuzzy PID controller has better robustness against disturbances due to the capability of adaptively tuning control gains (Xiang et al., 2017). The main disadvantage is that FLC needs existing experience to establish fuzzy rules, which is very subjective according to Zhang et al. (2019). In Londhe and Patre (2019), the authors proposed an adaptive fuzzy sliding mode control strategy for robust trajectory tracking control of an autonomous underwater vehicle.

Authors of Zhang et al. (2019) reported that the performance of the NNC depends on the architecture of the network, in particular on the number of nodes, resulting in a large computational cost, which is not conducive to the practical application of engineering (Yan et al., 2020), and therefore less applicable for underwater vehicles.

Authors of Tijjani et al. (2021) proposed a RAC control scheme for real-time control of a fully actuated AUV, including SMC as a control strategy, as it is a common motion control method used for controlling underwater vehicles (Yildiz et al., 2009; Londhe et al., 2017; Healey and Lienard, 1993; Elmokadem et al., 2016). The applicability of RAC and SMC is, in general, limited to AUVs as it involves complex controller design (Londhe et al., 2017). According to Hammad et al. (2017), SMC might lead to undesirable high-frequency oscillations called 'chattering' around the sliding surface, leading to low control accuracy and high energy consumption.

Authors of Budiyono (2011) proposed MPC as an alternative for direct-tuned PID controllers, as it is considered a promising control strategy for small underwater vehicles, such as AUVs.

Authors of Zhang et al. (2019) proposed a novel 3D underwater trajectory tracking method for a fully actuated AUV in 6 DOF leveraging MPC. They considered an MPC closed-loop optimal control strategy, reporting the capability of dealing with input and state constraints, while authors of Steenson et al. (2014) successfully applied MPC for transit and hovering control for the *Delphin2* AUV.

More recent research has been carried out to improve MPC for trajectory-tracking for underwater vehicles. In Yan et al. (2020), a double closed-loop controller is designed. In Long et al. (2021), the accuracy of MPC is further improved by using an extended state-based Kalman filter to estimate system states and external disturbances. The optimal control and corresponding propulsion force for each of the seven thrusters is determined for an ROV, considering the presence of ocean current disturbance and measurement noise (Long et al., 2021).

Authors of Tang et al. (2020) propose an improved kinematic MPC for high-speed path tracking of autonomous vehicles. The authors introduce a vehicle sideslip angle compensator to correct the kinematic model prediction, which significantly improves the performance of path tracking.

Authors of Tian et al. (2022) propose an adaptive path tracking control strategy that coordinates active front wheel steering and direct yaw moment based on the MPC algorithm. The authors use the recursive least square method with a forgetting factor to identify the rear tire cornering stiffness and update the path tracking system prediction model.

Authors of Xu et al. (2021) present a trajectory tracking scheme by utilizing MPC and preview-follower theory, which includes a reference generation module and a MPC controller. The authors claim that the proposed method performs well by increasing the effective length of the reference path.

Authors of Yu et al. (2021) carried out a review discussing the wide applications of MPC to both single and multiple autonomous ground vehicles. The authors highlight existing issues and future research directions, which will promote the development of MPC schemes with high performance in AGVs.

Table 1 provides a comprehensive summary of the advantages and disadvantages of each control method, as reported in the existing literature. The primary objective of this study is to introduce a novel control strategy, specifically designed to optimize the control and minimize the energy consumption of AUVs. Our research primarily concentrates on the aspect of Buoyancy Control, which involves the manipulation of the requisite mass in both the depth control tank and the forward trim tank. The distinguishing factor of our approach, as compared to traditional methods employed for remotely operated vehicles or AUVs, lies in the incorporation of a hopper within the hull. This addition results in a mass variation during underwater operations, necessitating active compensation. The novelty of our research is also encapsulated in its objectives. Unlike previous studies, our work does not solely focus on buoyancy control. Instead, it also aims to minimize energy requirements, thereby promoting cost-effectiveness and sustainability. This dual focus on control optimization and energy conservation sets our study apart, offering a fresh perspective on the control strategies for AUVs.

The control of an underwater dredger presents unique challenges compared to traditional underwater vehicles. Firstly, the operational state of an underwater dredger involves taking in liquid cargo while submerged. This process alters the vehicle's mass and buoyancy properties in real-time, adding complexity to the control problem. Traditional control strategies for underwater vehicles typically assume a constant mass and buoyancy, which is not the case for a dredger. Secondly, the dredger operates close to the seabed, which introduces additional physical constraints. The proximity to the ground can lead to ground effects, which are hydrodynamic changes that can affect the vehicle's

Table 1
Advantages and Disadvantages of different motion control methods for underwater vehicles.

Method	Advantages	Disadvantages
PID	Easy to implement, widely used, can be improved with adaptive tuning algorithms (Long et al., 2021; Sahoo et al., 2019; Rout and Subudhi, 2017; Kong et al., 2020; Xiang et al., 2017)	Less accurate for trajectory tracking and path following, unsuitable for nonlinear models and uncertain external disturbances, requires careful tuning (Zhang et al., 2019)
BSC	Used for controlling multi-input multi-output systems (Yan et al., 2020)	Cannot solve the uncertainty of system parameters and external disturbances, increased computing complexity with system order (Yan et al., 2020; Zhang et al., 2019)
FLC	Not dependent on an accurate mathematical model, can control uncertain and strong nonlinear systems, better performance and robustness against disturbances (Kong et al., 2020; Xiang et al., 2017)	Requires existing experience to establish fuzzy rules, which can be subjective (Zhang et al., 2019)
NNC	Improved performance compared to the physical model when implemented in the same feedforward-feedback control architecture (Zhang et al., 2019)	Performance depends on the architecture of the network, large computational cost (Zhang et al., 2019; Yan et al., 2020)
RAC and SMC	Used for real-time control of fully actuated AUVs (Tijjani et al., 2021)	Involves complex controller design, might lead to undesirable high-frequency oscillations (Londhe et al., 2017; Hammad et al., 2017)
MPC	Promising control strategy for small underwater vehicles, can deal with input and state constraints (Budiyono, 2011; Zhang et al., 2019; Steenson et al., 2014)	The performance of the MPC controller is highly dependent on the correct tuning of the weights in the cost function and the choice of the prediction horizon

stability and maneuverability. These effects are typically not a concern for vehicles operating in open water and at greater depths. Thirdly, the dredger must contend with currents affecting its trajectory and stability. While all underwater vehicles must deal with currents to some extent, the impact is more pronounced for a dredger due to its operational proximity to the seabed, where currents can be more turbulent. Lastly, the dredger often operates in shallow water, which introduces additional challenges. Shallow water effects, such as wave–current interactions and seabed boundary effects, can significantly impact the vehicle's dynamics and control.

Drawing from the existing body of literature, MPC emerges as a highly promising method for managing the motion control of underwater vehicles. This is largely due to its inherent ability to account for modeling uncertainties and external disturbances, while simultaneously optimizing the control effort. However, it is noteworthy that most of the research to date has primarily focused on applying MPC for buoyancy control. Our research aims to extend the application of MPC beyond this traditional focus. We propose an innovative approach that leverages MPC for buoyancy control and emphasizes energy minimization. This dual focus is designed to enhance the cost-effectiveness and sustainability of AUV operations. To our knowledge, this represents a novel contribution to the field, as no other research has yet explored the use of MPC in this manner. By broadening the application of MPC to include energy efficiency considerations, we aim to advance state-of-the-art AUV control strategies, potentially paving the way for more sustainable and economical underwater operations.

Therefore, this paper implements an MPC framework to achieve energy minimization whilst ensuring autonomous underwater operations. A PID-based control strategy is used to create a benchmark and compare the performance regarding trajectory-tracking and energy savings. The AUV under investigation (ALERD) has been modeled as an underwater vehicle using equations of motion and mathematical expressions for the hydrodynamic coefficients. Since it is a new unconventional building, no hydrodynamic data is available at the design stage, and for this reason, a sensitivity analysis has been carried out to show the effect of modeling uncertainties and the performance of both controllers. Finally, results are compared with the energy requirements of a conventional dredger to show the potential advantages of submerged dredging.

The rest of the paper is organized as follows.

Section 2 discusses the state-space modeling approach, the proposed MPC framework, and its numerical solution. Next, Section 3 outlines the derivation process of control forces and moments, subsequently translating these into corresponding power requirements and energy consumption. Section 4 describes the ALERD, including the tank arrangement and the disturbances due to the submerged dredging operations, used for the case study. In Section 5, the experimental settings are described. The results of the simulations will be presented in Section 6, using both PID control and MPC, and the results of the sensitivity analysis will be discussed. In Section 7, the comparison between the energy requirements of the ALERD and the conventional dredger is made. Finally, in Section 8, the conclusions will be given.

2. Methodology

In this section, we will deepen the description of the proposed methodology, starting from the state-space modeling approach presented in Section 2.1. Subsequently, in Section 2.2, we will describe the MPC framework considered for controlling the forward speed u, the pitch angle θ, and the depth z. This paper assumes that controlling the motions in heave and pitch will require the most energy for stability and buoyancy control. The energy consumption due to the forward speed control is based on the required power for propulsion, which is already determined in Hijdra and Van Der Harst (2019) and is not affecting the energy requirement for stability and buoyancy control. Furthermore, the disturbances due to the dredging and discharging operations will mainly influence the heave and pitch motion.

2.1. State-space modeling

The 6 degrees of freedom (DoF) model developed by Fossen (2011) is frequently used in the literature for the modeling of underwater vehicles and can be considered the state-of-the-art method for modeling and control of ships and underwater vehicles. According to Fossen (2011), the kinematic equations can be expressed in vectorial form

$$\dot{\boldsymbol{\eta}} = \mathbf{J}(\boldsymbol{\eta})\boldsymbol{\nu} \tag{1}$$

where $\boldsymbol{\eta} = [x, y, z, \phi, \theta, \psi]^T$ is the vector of position/Euler angles, $\boldsymbol{\nu} = [u, v, w, p, q, r]^T$ is the vector of velocities, and $\mathbf{J}(\eta)$ is the Euler transformation matrix.

The motions of the ALERD can be described using the complete equations of motion in 6 DoF as reported in Eq. (2):

$$\mathbf{M}\dot{\boldsymbol{\nu}} + \mathbf{C}(\boldsymbol{\nu})\boldsymbol{\nu} + \mathbf{D}(\boldsymbol{\nu})\boldsymbol{\nu} + \mathbf{g}(\boldsymbol{\eta}) = \boldsymbol{\tau} + \mathbf{w} \tag{2}$$

where $\mathbf{M} \in \mathbb{R}^{6\times6}$ is the system inertia and added mass matrix, $\mathbf{C}(\boldsymbol{\nu}) \in \mathbb{R}^{6\times6}$ is the Coriolis and centripetal matrix, $\mathbf{D}(\boldsymbol{\nu}) \in \mathbb{R}^{6\times6}$ is the damping matrix, $\mathbf{g}(\boldsymbol{\eta}) \in \mathbb{R}^{6\times1}$ is the vector with restoring forces and moments, $\boldsymbol{\tau} \in \mathbb{R}^{6\times1}$ is the vector with forces and moments applied to the vessel, and

w represents the external disturbances. It is worth noting that external disturbances have been neglected for this specific application. Eq. (2) can be rewritten as state-space representation, using the approach defined in Fossen (2011):

$$f(x,u) = \dot{x} = \begin{bmatrix} M^{-1}[\tau - C(\nu)\nu - D(\nu)\nu - g(\eta)] \\ J(\eta)\nu \end{bmatrix} \tag{3}$$

where $x = \begin{bmatrix} \nu^\top, & \eta^\top \end{bmatrix}^\top$ is the state vector. Exploiting the Euler transformation matrix, the velocity vector is transformed from the body-fixed to the inertial frame, according to Eq. (1).

Ideally, the hydrodynamic coefficients for the numerical simulations of the ALERD, based on Eq. (3), would have been retrieved using Experimental Fluid Dynamics (EFD) or Computational Fluid Dynamics (CFD). Those techniques can be considered state-of-the-art approaches to obtain the hydrodynamic coefficients required to capture the dynamic motions of the considered AUV described by Eq. (2). In fact, recent studies have been carried out developing CFD models to determine those coefficients for underwater vehicles (Gabriel et al., 2020; Gao et al., 2018; Takahashi and Sahoo, 2020) enabling the simulation of different maneuvers. Nonetheless, since the ALERD is still in the concept phase, both EFD or CFD-based approaches were impracticable.

Based on the literature, modeling the hull as an ellipsoid has been proven to be a good approximation of many slender body underwater vehicles and commonly used as reported in Fossen (2011), Lee et al. (2011) and Prestero (2001). Therefore, the hydrodynamic coefficients for the added mass are estimated, assuming the hull is ellipsoidal (Renilson, 2015; Severholt, 2017; Valeriano-Medina et al., 2013). Moreover, assuming three symmetry planes, the added mass and damping matrix become diagonal (Fossen, 2011). Furthermore, the higher-order damping terms can be neglected by assuming low to medium-speed operations (Fossen, 2011). The assumption of diagonal matrices can be considered a satisfactory approximation, since the off-diagonal coefficients are often much smaller compared to the diagonal coefficients (Fossen, 2011). By using diagonal matrices for the added mass and linear damping, the motions become almost decoupled.

The coefficients for the added mass are estimated using the k-factors from Lamb (Imlay, 1961), and the linear damping terms are scaled using data from a small AUV (Valeriano-Medina et al., 2013), using Froude scaling. Since the AUV used in Valeriano-Medina et al. (2013) and the ALERD have a similar Froude number, the Froude similarity is used. In general, Reynolds scaling is more applicable for the ALERD, due to the absence of waves. In submerged operations, viscous resistance is dominating. However, it is impossible to have Reynolds similarity between the small AUV and the ALERD. Therefore, it is chosen to scale the coefficients using the Froude scaling factors.

It is worth noting that the corresponding uncertainties induced by the estimations of the above-mentioned parameters have been considered, and sensitivity analysis has been performed and described in Section 5.1.

2.2. Model predictive control framework

The considered cost function is a sum over a prediction horizon of length (N_P), composed of two main contributions (Rawlings and Mayne, 2009).

For the first contribution, at each step in the horizon, the controller evaluates the difference between the predicted state of the system, denoted as $\eta(k+1)$, and the desired state, denoted as $\eta_d(k+1)$. This difference is then weighted by a positive-definite matrix $\boldsymbol{Q}$, assigning different weights to different state variables. The result is a measure of the tracking error of the system. The second term in the sum represents the control effort. It is the change in control input, denoted as $\boldsymbol{u}(k+i)$, weighted by a positive-definite matrix $\boldsymbol{R}$. This term penalizes large changes in the control input, which can be important in systems where abrupt changes in control can lead to instability or are otherwise undesirable (Kerrigan and Maciejowski, 2002). The controller seeks to minimize this cost function, which means it tries to find a sequence of control inputs that will result in the system closely tracking the desired state while minimizing the control effort. The proposed cost function represents a trade-off between tracking performance (how closely the system follows the desired trajectory) and control effort (how much the control input changes), and the matrices $\boldsymbol{Q}$ and $\boldsymbol{R}$ are used to tune this trade-off.

The cost function is quadratic (see Eq. (4)), which means the problem is a Quadratic Programming (QP) problem if the system dynamics and constraints are linear (Boyd and Vandenberghe, 2004). QP problems can be solved efficiently, which is one of the reasons why MPC is popular for controlling linear systems. Nonetheless, our system is a nonlinear one, therefore, the problem becomes a Nonlinear Programming (NLP) problem, which is more challenging to solve (Guo et al., 2017). Optimality and stability are fundamental properties sought in the control of linear and nonlinear systems using MPC, which explains the rationale for minimizing the cost function (Mayne et al., 2000).

In particular, the cost function of the MPC is defined by Eq. (4). Within this equation, the matrices $\boldsymbol{Q} \in \mathbb{R}^{2\times2}$ and $\boldsymbol{R} \in \mathbb{R}^{2\times2}$ are characterized as positive-semi-definite, representing the weight parameters within the function. The cost function's objective is to accurately track the desired reference signals, namely the depth z and pitch angle θ, while simultaneously minimizing the adjustments in the manipulated variable, Δu. These control objectives encapsulate the MPC's key goal and are defined more precisely in Eq. (5). The manipulated variables, namely the required mass in the depth control tank (DCT) (m_{DCT}) and the required mass in the forward trim tank ($m_{TT,fore}$), are central to the controller's operation and are thoroughly defined in Eq. (6).

$$J = \min \sum_{i=0}^{N_p} \Big(\big(\boldsymbol{\eta}(k+i) - \boldsymbol{\eta_d}(k+1)\big)^T \boldsymbol{Q} \big(\boldsymbol{\eta}(k+i) - \boldsymbol{\eta}_d(k+1)\big) + \Delta\boldsymbol{u}(k+i)^T \boldsymbol{R} \Delta\boldsymbol{u}(k+i) \Big) \tag{4}$$

with

$$\boldsymbol{\eta}_d(k+i) = \begin{bmatrix} z_d(k+i) \\ \theta_d(k+i) \end{bmatrix} \tag{5}$$

$$\boldsymbol{u}(k+i) = \begin{bmatrix} m_{DCT}(k+i) \\ m_{TT,fore}(k+i) \end{bmatrix} \tag{6}$$

The variation in the manipulated variable, computed via Eq. (7), establishes the rigid constraint for the controller's operation. This specific constraint, detailed in Eq. (8), is equivalent to the mass flow rate as determined by Eq. (9). This hard constraint is fundamentally derived from the inherent properties of the physical system in use, namely the ballast water pump system. Given certain parameters, such as the pipe diameter for each tank system and a predefined maximum flow velocity in the pipeline, it becomes possible to discern a maximum volume flow rate and its correlative mass flow rate. These values, once defined, are employed to limit the range within which the controller can operate. This aspect of the system ensures that the controller remains within the safe and effective operating parameters of the ballast water pump system.

$$\Delta\boldsymbol{u}(k+i) = \boldsymbol{u}(k+i \mid k) - \boldsymbol{u}(k+i-1 \mid k) \tag{7}$$

$$\Delta\boldsymbol{u}_{min} \leq \Delta\boldsymbol{u}(k+i) \leq \Delta\boldsymbol{u}_{max} \tag{8}$$

$$\dot{m}_{max} = \rho_{sw} \cdot v_{max} \cdot \frac{\pi}{4} \cdot d_{pipe}^2 \tag{9}$$

The required mass flow rate directly relates to the necessary pump power as exhibited in Eq. (12). Optimizing the change in the manipulated variable – that is, the mass flow rate – is intrinsically linked with optimizing the power requirement for the ballast water pumps.

2.3. MPC numerical solution

The numerical solution of this MPC problem involves solving the optimization problem defined by the cost function described in Eq. (4) at each time step. The goal is to find the optimal control inputs $\boldsymbol{u}$ that minimize this cost function. Since our system is a nonlinear one, the problem becomes a Nonlinear Programming (NLP) problem, which is more challenging to solve (Guo et al., 2017). To solve such an NLP problem, the literature suggests a number of numerical optimization methods: (i) Gradient-based methods: these methods use the gradient (or derivative) of the objective function to guide the search for the optimal solution. They start with an initial guess for the solution and iteratively update this guess in the direction that decreases the objective function the most. Examples of gradient-based methods include steepest descent, conjugate gradient, and Newton's method (Nocedal and Wright, 1999). (ii) Sequential Quadratic Programming (SQP): SQP is a popular method for solving NLP problems. It works by approximating the NLP problem with a sequence of QP problems. The QP problems are easier to solve, and the solutions to these problems converge to the solution of the NLP problem (Fletcher, 1981). (iii) Interior-point methods transform the NLP problem into an equivalent problem that can be solved more easily. They do this by introducing a barrier function that prevents the search from reaching the boundaries of the feasible region (Biegler, 2010). (iv) Genetic algorithms or other evolutionary algorithms: these are population-based, stochastic search algorithms inspired by natural evolution principles. They can be used to solve optimization problems, including NLP problems, especially when the objective function is non-convex or has multiple local minima (Goldberg, 1989). In our study, we have chosen SQP as our method for solving the nonlinear programming problem. The justification lies in its efficacy for complex problems, convergence properties, and ability to handle constraints. SQP is adept at tackling the intricate optimization problems that come with marine vehicle control, which often involve numerous variables and constraints (Nocedal and Wright, 1999). The performance of marine vehicles can be swayed by a multitude of factors, such as vehicle dynamics, hydrodynamic forces, and environmental conditions (von Ellenrieder, 2021; Karimi and Lu, 2021). These factors contribute to a complex optimization problem, which SQP is well-equipped to manage. In terms of convergence properties, SQP methods are known for their robustness, with solutions tending to converge swiftly and reliably to the solution of the nonlinear programming problem (Nocedal and Wright, 1999). This is particularly beneficial in the context of marine vehicle control, where solutions may be required in real-time or near-real-time. Lastly, marine vehicles often operate under a variety of constraints, such as limitations on thruster power or navigational restrictions. SQP proves effective at managing these types of constraints in the optimization problem (Fossen and Strand, 1999).

In each iteration of the MPC algorithm, the QP solver will take the system's current state and the reference trajectory for the future N_p steps and return the optimal control inputs that should be applied to the system. The first input of this optimal sequence is applied to the system, and the process is repeated at the next time step. The matrices $\boldsymbol{Q}$ and $\boldsymbol{R}$ in Eq. (4) are used to tune the performance of the MPC controller. The matrix $\boldsymbol{Q}$ weights the tracking error (the difference between the system states and the desired reference), while the matrix $\boldsymbol{R}$ weights the change in control inputs. Adjusting these weights allows us to control the trade-off between tracking performance and control effort. The solution of the QP problem will give us the optimal values for the manipulated variables, m_{DCT} and $m_{TT,fore}$, as defined in Eq. (6). These variables are the key operational parameters that our controller can adjust to track the desired depth and pitch angle, as the reference signals specify. Using a QP solver allows us to systematically and efficiently find the solution to our MPC problem. However, the performance of the MPC controller is highly dependent on the correct tuning of the weights in the cost function and the choice of the prediction horizon N_p.

3. Energy assessment

In this section, the required control forces and moments defined in Section 3.1 are derived and subsequently translated into the required power and corresponding energy consumption as reported in Section 3.2.

3.1. Control forces and moments

The control variables are employed to generate the necessary restoring forces and moments as explicated in Eqs. (10) and (11). Two integral components – the depth control tank and the trim tank system – are exploited to produce these restoring forces and moments. The trim tank system has been modeled considering that the mass extracted from the forward tank is concurrently added to the aft tank and reciprocally. This approach ensures that the total mass within the trim tank system remains conserved. The heave force and the trimming moment are incorporated within the force vector $\boldsymbol{\tau} \in \mathbb{R}^{6\times1}$, as defined in Eq. (3). It is assumed that the DCTs are positioned so that they do not create additional trimming moments, so adding or removing weight only creates additional forces in heave motion. Furthermore, it is assumed that the center of gravity does not change, meaning the vertical distance from the center of buoyancy (B) to the center of gravity (G) remains constant. Adding or removing mass from the DCT can generate negative and positive forces. In the case of underwater vehicles, the application of negative forces becomes necessary for ascent. This is primarily because the weight (W) of the vehicle must be less than the buoyant force (B) for the vehicle to rise. In Eq. (10), the heave force due to the mass in the DCT can be found.

$$\mathrm{F_{DCT}} = g \cdot m_{DCT} \tag{10}$$

In this study, the authors have resolved not to employ stern-planes as actuators for pitch control, a decision mirroring that adopted in naval submarine designs. Rather, a trim tank system has been selected as the method for managing pitch. The ALERD's trim tank system is a closed configuration comprising two interconnected tanks. These tanks are strategically positioned 30 m apart, both fore and aft, relative to the central origin point (CO), denoted as $x_{TT,fore}$ and $x_{TT,aft}$ in the longitudinal direction. Thanks to the symmetric positioning of the tanks, no supplemental trimming moments are generated in either the pitch or roll direction. This ensures a balanced, effective system for pitch control.

A more elaborate discussion on the arrangement of the trim tanks will follow in Section 4.1, including a schematic depiction of the tank layout within the hull, as illustrated in Fig. 4, to provide a detailed understanding of the system's design.

Keeping this in view, the trim tanks play a crucial role in generating necessary restoring moments, ensuring consistent zero-pitch control. The mass to be inserted or extracted from the forward trim tank ($m_{TT,fore}$) is the pitch angle's control variable. This mass is converted into a trimming moment, which then serves as an input in the forces and moments vector τ, as represented in the state-space Eq. (3).

The trimming moments ($M_{TT,fore}$ and $M_{TT,aft}$), as a product of the trim tank system, are detailed in Eq. (11).

$$\begin{aligned} M_{TT,fore} &= g \cdot x_{TT,fore} \cdot \left(\frac{m_{TT,tot}}{2} + m_{TT,fore}\right) \\ M_{TT,aft} &= g \cdot x_{TT,aft} \cdot \left(\frac{m_{TT,tot}}{2} - m_{TT,fore}\right) \end{aligned} \tag{11}$$

3.2. Depth and pitch control energy assessment

The required mass flow for the ballast tanks used for depth- and pitch control and to compensate for the weight in the hopper can be used to calculate the required pump power and corresponding energy consumption. When the tanks need to be emptied, pumps are used, and if they need to be filled, flooding holes are opened. Therefore,

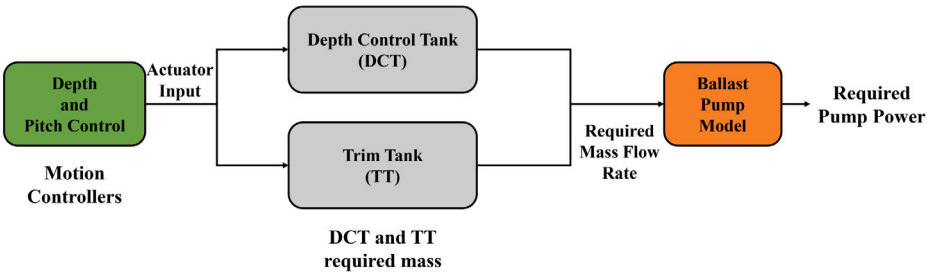

Fig. 1. Energy consumption flow chart.

only the negative mass flow (i.e., water removed from the tanks) is considered when calculating the pump power. Positive mass flow rates are achieved by opening vents, which do not contribute to energy consumption. The mass flow rate is constrained based on the maximum fluid flow velocity in the pipelines, which is already described in Section 2.2. The mass flow rate is then converted to a volume flow rate, which serves as input for calculating the required power by the pumps, using Eq. (12). This is also schematically drawn in Fig. 1. In Eq. (12), $\dot{V}_{pump}$ is the volume flow in m^3/s and η_{pump} the pump efficiency. Values for the pump efficiency for centrifugal pumps vary between $[0.6, 0.9]$ and are dependent on the pressure head. The total pressure head (Δp^{++}_{pump}) includes the static pressure head, the dynamic pressure head, and the head caused by a height difference in the pipe-flow system itself.

$$P_{B,pump} = \frac{\dot{V}_{pump} \cdot \Delta p^{++}_{pump}}{\eta_{pump}} \tag{12}$$

Once the required pump power is evaluated, we can calculate the total energy requirement in kilojoules (kJ) for a single simulation run. This is achieved by integrating the power over the entire simulation duration. Detailed comparative analysis can be found in Section 7.

4. Case study description

In this paper, we utilize ALERD as the focal point of our case study. We aim to demonstrate the potential advantages of integrating autonomous submerged dredging operations with the proposed MPC framework. This section will detail an exhaustive characterization of the ALERD. We will describe its primary architectural dimensions and the internal configuration of the tank system within the hull. This in-depth analysis will afford a thorough understanding of the structural parameters and functional aspects influencing the performance of ALERD. Moreover, we will explore the disturbances that are intrinsic to submerged operations. These disturbances, which present challenges in the practical implementation of the system, will serve to underscore the robustness and resilience of the proposed MPC framework when confronted with real-world operational conditions. This comprehensive analysis will allow a more robust understanding of the theoretical and practical implications of employing the proposed MPC framework in autonomous submerged dredging.

4.1. Vessel description

The ALERD is an autonomous submersible dredger that is designed to deliver sediment to coastlines to protect the land in a sustainable manner. The ALERD's autonomous operation and sustainable power source make it a more environmentally friendly option than traditional dredgers, as it is powered by a battery and uses a combination of sensors and software to navigate and operate autonomously. This makes the ALERD a more sustainable option than traditional dredgers, which are typically powered by diesel fuel. The ALERD's ability to operate in shallow waters makes it ideal for coastal replenishment projects. The ALERD uses a suction dredge to collect sediment from the seabed, and the sediment is then transported to a hopper in the ALERD's hull. The vehicle uses its thrusters to navigate to the desired location, where the sediment is then discharged from the hopper onto the coastline. The ALERD is designed to be operated autonomously, meaning it does not require a crew to operate it. The sensors include sonar, GPS, and a compass. The software uses the data from these sensors to map the surrounding area and plan the ALERD's movements.

Table 2
Wageningen B3-65 nozzle 19A main characteristics.

Feature	Symbol	Value	Unit
Propeller diameter	D_{prop}	2.8	[m]
Trust coefficient	K_T	0.207	[–]
Torque coefficient	K_Q	0.0297	[–]
Number of propellers	n_p	2	[–]

Given that the ALERD is still in its conceptual phase, the definitive dimensions and hull form remain indeterminate. However, a preliminary hull form, illustrated in Fig. 2, has been proposed. This preliminary hull form derives its foundation from prior research work (Hijdra and Van Der Harst, 2019), as well as from the ALERD's predecessor — the Autonomous Underwater Maintenance Dredger (AUMD). A comprehensive description of the AUMD, along with its distinctive attributes, is available in Hijdra and Van Der Harst (2019). The propulsion system of the ALERD encompasses two azimuthing thrusters, which are designed to function as primary propulsors. In addition, batteries are incorporated to provide the necessary energy on board. The specifications of the propellers, which form a crucial component of the propulsion system, are enumerated in Table 2.

Fig. 3 presents a cross-sectional view of the hull. The hopper, which is used for storing the excavated soil, is strategically positioned within the hull. The flooding holes situated at the top of the hopper are clearly delineated in Figs. 2 and 3. ALERD is designed with bottom-door openings at the hull's base to facilitate the discharge of the dredged soil. The hopper is consistently filled either with seawater or a mixture of seawater and the excavated soil. Throughout the dredging operations, the dredged material is transferred into the hopper using specialized dredging pumps. The upper flooding holes have been designed to serve a dual purpose: they can be used either to drain excess water or to fill the hopper with seawater. Similarly, the bottom-door openings function to discharge the dredged soil. Key dimensions of the ALERD are provided in Table 3. The dimensions and displacement correspond to the hull form of its predecessor, the AUMD, as shown in Fig. 2. The initial dimensions of the AUMD serve as the foundational reference for the ALERD and are consistently utilized in this research. Given the operational differences between the ALERD and the AUMD, further optimization of these dimensions will be necessary and will be the focus of future research. The hopper capacity is deduced based on the primary dimensions of the hull and previous studies conducted on the ALERD. These hopper dimensions, in turn, are employed to determine the ballast capacity of the primary ballast tanks.

The arrangement of the three ballast tank systems and the hopper is depicted in Fig. 4. The depth control tank (DCT) is employed as

Fig. 2. Preliminary hull form.

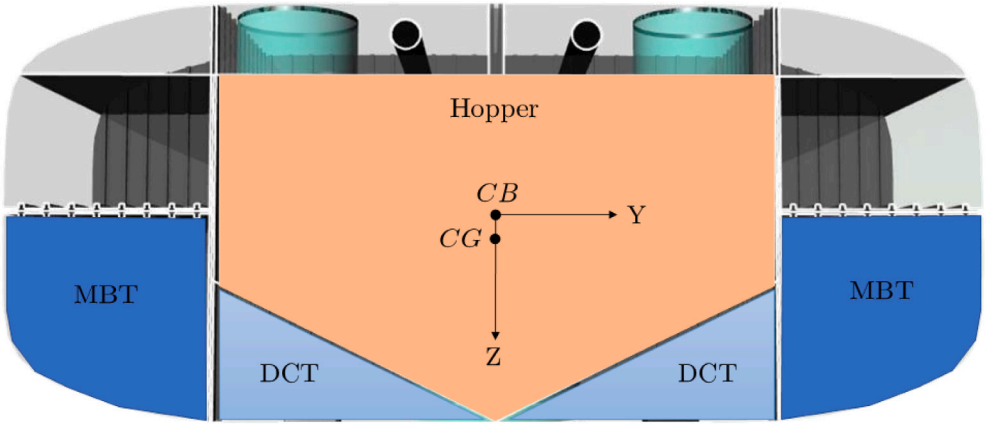

Fig. 3. Schematic overview of the cross-section of the hull.

Table 3
Main dimensions.

Parameter	Symbol	Value	Unit
Length	L	80	[m]
Breadth	B	20	[m]
Depth	D	8.5	[m]
Displacement	Δ	10 830	[ton]
Hopper volume	∇_H	2360	[m^3]

an actuator for the motion controller, enabling the active control of the depth z. Similarly, the trim tanks situated at the forward and aft sections of the hull serve as actuators for the motion controller, enabling the control of the pitch angle θ. The two tank systems are instrumental in generating the requisite control forces and moments, as outlined in Section 2. Fig. 3 provides a cross-sectional view of the hull, showcasing the arrangement of the tanks and the hopper. The weights associated with the hopper and the main ballast tanks (MBTs) are detailed in Table 4.

During dredging operations, the hopper is filled with a mixture of the dredged soil and seawater, which has a density denoted by $\rho_{mix} = 1900\ \mathrm{kg/m^3}$. The MBTs are employed to counterbalance this weight change and, consequently, possess the same capacity as the additional weight introduced into the hopper. This capacity is also specified in Table 5. The design and operation of these systems are meticulously planned to ensure efficient dredging while maintaining vessel stability.

Table 4
Hopper and tank mass details.

Parameter	Value	Unit
Hopper mass (Water)	$2419 \cdot 10^3$	[kg]
Hopper mass (Mixture)	$4484 \cdot 10^3$	[kg]
Mass main ballast tank	$2065 \cdot 10^3$	[kg]

Table 5
Parameters trim tank system.

Parameter	Value	Unit
$x_{TT,aft}$	30	[m]
$x_{TT,fore}$	30	[m]
$m_{TT,tot}$	10 000	[kg]

4.2. Disturbances

Fig. 5 illustrates the changes in the mass of the hopper and the main ballast tank over time. It is assumed that the filling of the hopper with dredged soil and the emptying of the main ballast tanks occur simultaneously and at equivalent mass flow rates. This hypothesis guarantees that the mass differential between the main ballast tank and the hopper during both dredging and discharging operations remains null at all instances, a phenomenon corroborated by Fig. 5. By adhering to this approach, the generation of additional heave forces is avoided, thereby eliminating the need for further compensation. Consequently, the depth control tank is utilized exclusively for implementing necessary depth

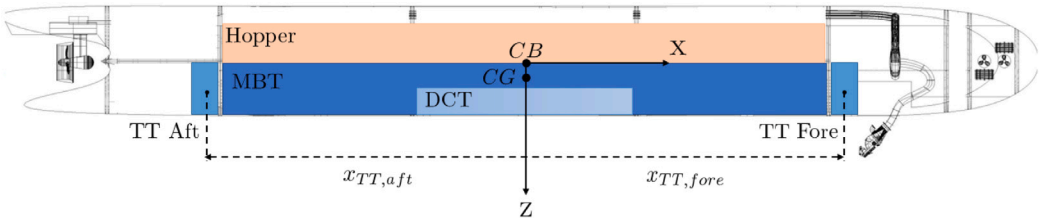

Fig. 4. Schematic overview of the hopper and the tank arrangement.

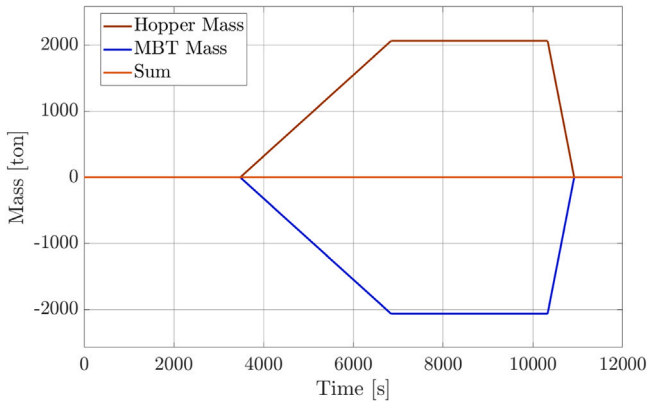

Fig. 5. Mass change in the hopper and MBT.

adjustments, while the main ballast tank is devoted to offsetting the mass variations in the hopper. This strict partition of responsibilities ensures the stabilization of the vessel during its operations, enhancing the efficiency of the dredging process.

During the dredging operation, one of the significant disturbances arises from the resistance of the draghead and suction tubes. The calculation of this resistance for a traditional dredger can be applied to the ALERD due to the similar size and quantity of dragheads used — in this case, two. It is assumed that the resistance exerted by the dragheads on the ALERD is equal to that on a conventional dredger due to their similar design and operational parameters. The forward speed during dredging, set to a constant 2 knots, results in an estimated resistance from the two dragheads equal to 258 kN, while the resistance attributed to the suction tubes amounts to 2 kN. These resistances sum up to a total of 260 kN, which introduces a constant trimming moment during the dredging operation. This induced moment necessitates active compensation from the trim tanks to maintain a zero pitch angle, thus ensuring the stability of the vessel during operations. This analysis underscores the importance of accounting for such disturbances in the design and control strategies for autonomous dredgers like the ALERD.

5. Experimental setting

In this section, we introduce the experimental settings for our study, where we consider a realistic speed profile reflecting the operational habits of conventional dredgers engaged in coastal replenishment activities along the Dutch coastline. This choice is made to create scenarios that closely resemble real-world operations.

The forward speed during transit, dredging, and discharging is set at 8.5 knots, 2 knots, and 0.4 knots, respectively. This variation in speed profile serves as an input for the state-space model, making the simulation more robust and representative of practical conditions.

The calculation of thrust and torque, as formulated in Eqs. (13) and (14), are incorporated into the force vector $\boldsymbol{\tau} \in \mathbb{R}^{6\times1}$ (referenced in Eq. (3)). These calculations rely on the propeller characteristics, detailed in Table 2 within Section 4.

$$T = 0.5 \cdot \rho \cdot D_{prop^4} \cdot K_T \cdot n^2 \tag{13}$$

$$Q = 0.5 \cdot \rho \cdot D_{prop^5} \cdot K_Q \cdot n^2 \tag{14}$$

where n is the propeller speed, and it plays a critical role in the functioning of the motion controllers, as it is instrumental in achieving the desired vessel speed. This experimental setting serves to provide a comprehensive evaluation of the vehicle's performance under realistic operational conditions.

In this section, we employ the state-space model delineated in the preceding segment to conduct time-domain simulations over the span of one complete dredging cycle. This approach facilitates a thorough understanding of system dynamics throughout a full operational cycle. Two control methodologies, namely PID control and MPC, are incorporated into the simulation model. The aim of these controls is to meet the defined control objectives while simultaneously addressing any disturbances encountered during dredging and discharging operations. In terms of energy consumption, the main contributors are the tank systems (MBT, DCT, and TTs), which play a pivotal role in ensuring stability and controlling buoyancy. These tank systems, acting as actuators, are utilized by the motion controllers to meet the control objectives specified earlier. The DCT and TTs, in particular, are active components in this control scheme, responding to the controller's commands to adjust the vessel's dept (compensating for salinity and hull compression) and pitch angle. By analyzing their role in the context of the entire dredging cycle, we aim to gain insights into the system's behavior and identify potential areas for energy efficiency improvement. This also aids in understanding how variations in these parameters influence the overall performance and energy requirements.

Fig. 6 depicts the prescribed depth trajectory. This reference signal maps the desired position of the center of origin (CO), which coincides with the center of buoyancy (CB). Notably, all the forces and moments in the system are expressed with respect to this reference point. The operational profile exhibited in Fig. 6 is derived from the median values of numerous operational profiles from conventional dredgers performing coastal replenishment activities along the Dutch coastline. These profiles were obtained via an analysis of data from the Automatic Identification System (AIS). In this context, the maximum water depth is postulated to be 21 m, an assumption rooted in the operational profile analysis. The figure distinctly outlines the three operational modes: transit, dredging, and discharging. During transit operations, the vehicle is designed to maintain a depth of 8 m. During dredging operations, this depth is adjusted to 15 m to facilitate efficient soil extraction. Subsequently, during discharging operations, the vehicle is required to ascend to a depth of 4 m, enabling an effective release of the dredged material. These depth adjustments are integral to the operational efficiency and energy management.

The target for the pitch angle is to maintain a value of zero degrees at all times. This decision is informed by a balance of the structural length of 80 m and the maximum operational water depth of 21 m. Maintaining a zero-degree pitch angle ensures optimal operational stability and efficiency in this context. The parameters defining the operational modes, such as velocity, depth, and duration, are designed to be analogous to those of conventional dredgers. This strategic similarity enables a direct comparison of energy requirements between the

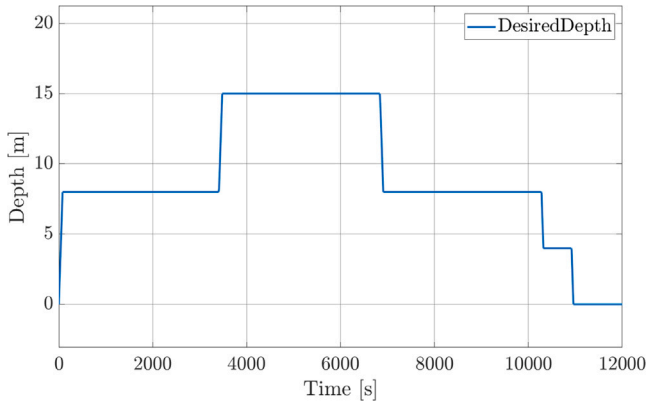

Fig. 6. Reference signal for the vertical position.

ALERD and conventional systems, thereby providing a robust measure of the relative performance and efficiency.

Simulation runs are executed employing the designated reference signals for both the pitch angle (θ) and depth (z), with PID control serving as the benchmark for controller performance. The innovative MPC strategy proposed in this study is then implemented, and its performance is evaluated relative to the PID benchmark. One key aspect of the comparative analysis lies in measuring the corresponding energy requirements under both control strategies. To ensure a balanced comparison, the ALERD MPC-controlled is juxtaposed with a conventional dredger of similar hopper volume and operational profile. This comparison aims to elucidate whether the MPC offers any advantages in terms of energy consumption relative to both the conventional dredger and the PID. In the following section, the outcomes of these simulation runs and comparative analyses will be explored and discussed in detail.

5.1. Sensitivity analysis

To quantitatively analyze the impact of modeling uncertainties on the results of time-domain simulations, a comprehensive sensitivity analysis is undertaken. The process of creating a state-space model replete with hydrodynamic coefficients inherently introduces certain uncertainties. These uncertainties primarily stem from the linear damping coefficients, which are scaled, and the assumption of an ellipsoidal hull-form for the computation of the added mass coefficients. Such uncertainties are inherent in the mathematical modeling of an underwater vehicle, and accounting for them is a critical component of the simulation model's effectiveness. The sensitivity analysis aims to quantify the impact of these uncertainties on the model's predictive accuracy and robustness. This procedure not only tests the robustness of the control strategy, but also provides valuable insights into potential areas for model refinement and improvement. This level of analysis is crucial as it can uncover potential limitations or weaknesses within the model, thereby informing future research and development efforts. It also assists in understanding the degree to which these uncertainties may impact the overall efficacy of the proposed MPC strategy for autonomous submerged dredging. In the next section, the outcomes of this sensitivity analysis will be thoroughly discussed.

To thoroughly evaluate the influence of model input uncertainties on the outputs, and to assess the robustness of the control schemes, we employ a Monte Carlo simulation methodology. This technique is a class of computational algorithms that rely on repeated random sampling to achieve numerical results, hence providing a probabilistic means to assess the uncertainties in the system. The specific coefficients selected for the uncertainty analysis are detailed in Table 6. Each of these coefficients is presumed to have an uncertainty of 20%. In the context of this analysis, we assume that the calculated value of each coefficient represents its mean value, denoted by μ. The corresponding standard deviation, denoted by σ, is derived from the aforementioned 20% uncertainty assumption. It should be noted that the choice of a 20% uncertainty is somewhat arbitrary and serves as a generic assumption for the purpose of this analysis. This level of uncertainty was selected to provide a sufficiently broad range of potential values, thus ensuring the robustness of the results to variations in these coefficients. The Monte Carlo simulation is then implemented, using these mean values and standard deviations, to generate a distribution of possible outcomes. This allows for a comprehensive analysis of the system's behavior under varying conditions, and provides insights into the stability and performance of the control strategies under uncertainty. The results of this simulation will be presented and discussed in the subsequent section.

Table 6
Mean and standard deviation of the chosen coefficients.

Coefficient	Unit	Mean	Standard deviation
Z_w	[N/(m/s)]	$2.54 \cdot 10^5$	$1.69 \cdot 10^4$
M_q	[(N m)/(rad/s)]	$1.35 \cdot 10^8$	$9.02 \cdot 10^6$
$Z_{\dot{w}}$	[kg]	$9.7 \cdot 10^6$	$6.46 \cdot 10^5$
I_{yy}	[kg m^2]	$3.6 \cdot 10^9$	$2.4 \cdot 10^8$
η_{pump}	–	0.725	0.048
ζ	–	70	4.67

The primary control objectives in our model are the management of pitch and depth, which are directly influenced by several coefficients within the equations of motion in these two DoF. Specifically, alterations in added mass or damping coefficients could induce significant changes in the resulting motions along these axes. This makes these coefficients particularly suitable for assessing the performance and robustness of the control mechanisms under investigation. It is, however, essential to note that the ALERD, in our model, is approximated as an ellipsoid. This simplification has implications for the calculated values of the moments of inertia, as they do not perfectly reflect the moments of inertia corresponding to the actual hull form of the ALERD. While this approximation aids in the computational tractability of our model, it also introduces an inherent source of error, further emphasizing the importance of conducting an uncertainty analysis. By incorporating this level of variability into our analysis, we can more accurately assess the effectiveness of the control strategies in a realistic, non-idealized setting. This not only enhances the robustness of our findings, but also provides valuable insights into the performance of the controllers in the face of real-world uncertainties and challenges.

Therefore, the following coefficients have been considered as the main source of uncertainties:

- Z_w: Linear damping coefficient in heave (z)
- M_q: Linear damping coefficient in pitch (θ)
- $Z_{\dot{w}}$: Added mass coefficient in heave (z)
- I_{yy}: Mass moment of inertia in y-direction.

Two additional coefficients, as listed below, are subjected to random distribution due to their direct impact on the energy requirement calculations. These particular coefficients are selected due to the inherent uncertainty surrounding their actual values. The efficiency of the pumps (η_{pump}) typically falls within the range of 0.6 to 0.9 for conventional ships, while the flow resistance coefficient (ζ) can vary between 10 to 100. The specific details about the pumps to be utilized and the exact layout of the onboard pipeline system for the ALERD are not currently available. This lack of detailed information further underscores the importance of accounting for variability in these coefficients. Incorporating this range of uncertainty in our model allows us to anticipate and plan for a broader spectrum of potential real-world conditions and outcomes.

- η_{pump}: Centrifugal pump efficiency;
- ζ: Resistance factor.

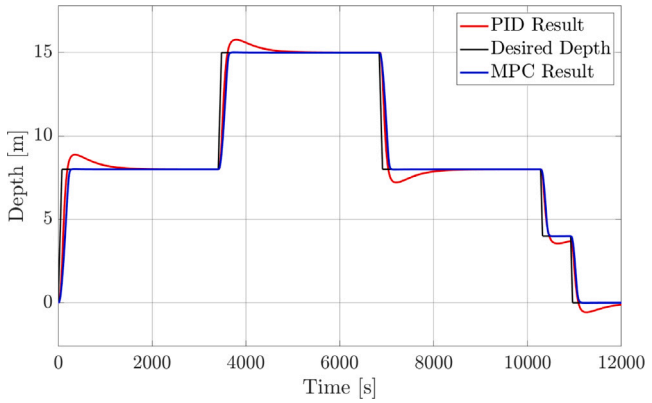

Fig. 7. PID and MPC depth control comparison.

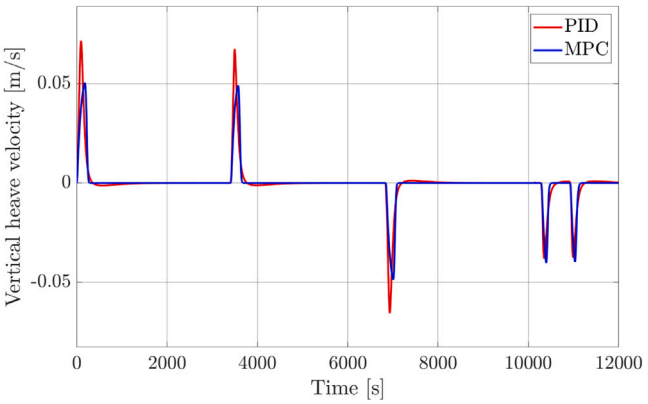

Fig. 8. PID and MPC heave velocity comparison.

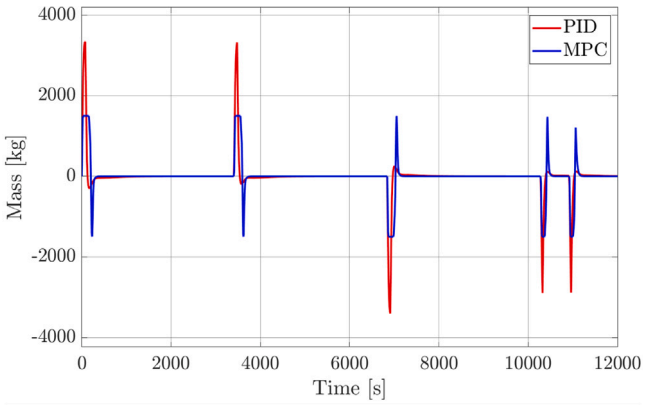

Fig. 9. PID and MPC required DCT mass comparison.

The parameters μ and σ are deployed to generate 10,000 random samples conforming to a normal distribution for each of the six coefficients. These extensive, normally distributed samples enable a thorough exploration of potential parameter variability. From each of these normally distributed datasets, a smaller sample of 1000 random numbers is selected to serve as inputs for the simulation. This process results in 1000 unique combinations of the six coefficients, each set representing a different potential realization of model parameters. The large number of samples enhances the robustness of our statistical analysis, thereby increasing the reliability and generalizability of the results.

6. Results and discussion

In this section, we present the results of the time-domain simulations using both PID controllers and the proposed MPC strategy (Section 6.1). The performance of the controllers is evaluated based on their ability to achieve the desired control objectives, namely pitch and depth control, and their energy consumption. Next, in Section 6.2 the results of the sensitivity analysis are presented to assess the effect of modeling uncertainties on the outcomes of the simulations.

6.1. Simulation results

In Fig. 7, the results of tracking the desired depth signal, as shown in Fig. 6, are presented. A comparison between the performance of the PID controller and MPC reveals that MPC exhibits superior tracking of the reference depth, with significantly reduced overshoot compared to PID. This improvement in performance is also reflected in Table 8, where a reduction in energy consumption for controlling depth can be observed. This is attributed to the behavior and control effort of the controllers. Furthermore, Fig. 8 compares the vertical heave velocity under the control of PID and MPC.

Fig. 9 displays the required mass in the DCT for both controllers. MPC requires more negative mass (i.e., ballast mass removed from the tanks) when the ALERD is diving to its reference depth. This leads to a negative upward force that decelerates the vehicle during the descending phase, resulting in a smaller vertical velocity compared to the results obtained with the PID controller, as shown in Fig. 8. Conversely, if the vehicle is ascending to its new reference depth, MPC demands more added ballast mass in the tanks than the PID controller, which again decelerates the motion, thereby reducing the overshoot of the desired signal. The effect of the added and removed mass in the DCT on the vertical heave velocity w can be observed in Fig. 8. Specifically, the vertical velocity for the PID controller is higher and remains so for a longer period during the peaks, which leads to the overshoot of the desired depth. For the MPC controller, this velocity is smaller due to the braking effect of the mass in the DCT. Therefore, the output of the MPC controller enables to achieve better reference tracking compared to the PID controller.

The vertical movement during the descending (or ascending) is slowed down more aggressively by MPC, leading to almost no overshoot, while optimizing the control outputs. This can be explained by looking at Fig. 10. In this figure, it is clear that the mass flow rate is constrained for both controllers. This constraint is chosen based on the physical systems, which are the ballast water pump system, including the pipe-flow systems. It is assumed that the physical constraint is the fluid velocity in the pipeline, which in combination with a chosen pipe diameter, constrains the mass flow rate. Although similar maximum values for the mass flow rate are reached, the duration of the maximum mass flow rate for the PID controller is larger compared to MPC. The energy consumption, corresponding to the mass flow rates from Fig. 10, can be seen in Fig. 11. From this figure, it can be concluded that using MPC, reduces the required energy consumption for controlling the depth. The MPC controller output, the required mass in the tanks, leads to almost perfect reference tracking due to the reduced vertical velocity while at the same time minimizing the energy requirements.

In Fig. 12, the comparison is shown of the reference tracking from the desired pitch angle θ. It is clear that the MPC's maximum deviation is larger compared to the PID controller. Due to the significant disturbance of the draghead, shown in Fig. 13, extensive control actions must take place to keep the pitch angle zero. For the pitch controller, reducing aggressive control moves and minimizing the control effort is prioritized over perfect reference tracking, using the weight matrices $\boldsymbol{Q}$ and $\boldsymbol{R}$ from Eq. (4). It turned out that aggressive control moves lead to a significant increase in energy consumption, while the order

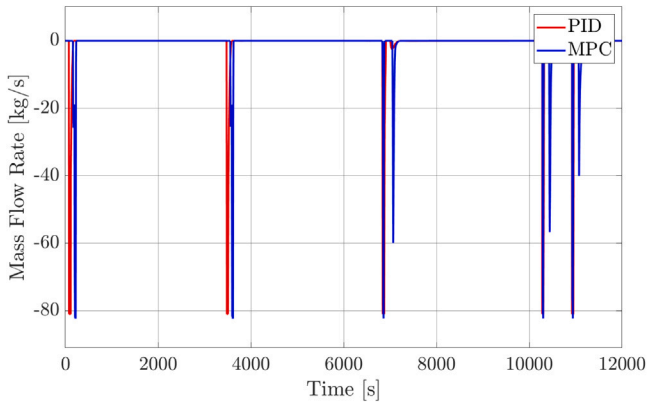

Fig. 10. PID and MPC required DCT mass flow rate comparison.

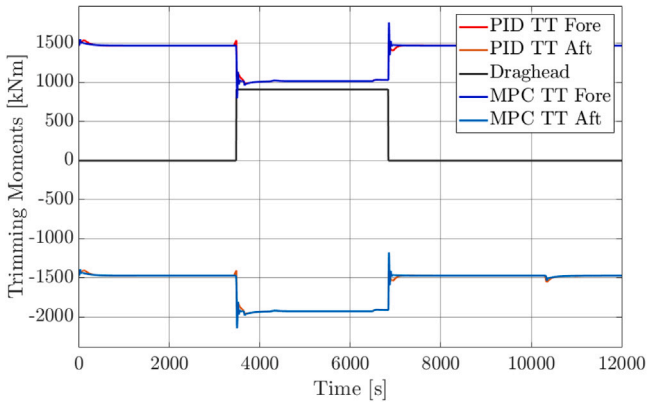

Fig. 13. PID and MPC trimming moments comparison.

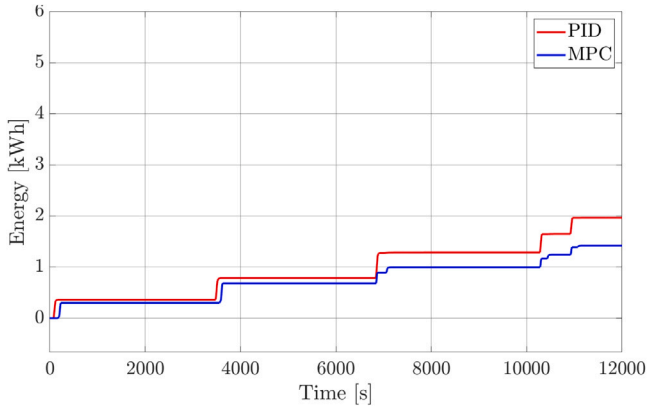

Fig. 11. PID and MPC DCT energy consumption comparison.

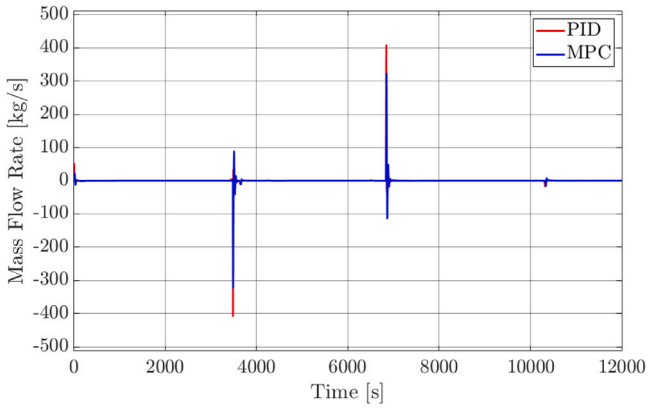

Fig. 14. PID and MPC required TT mass flow rate comparison.

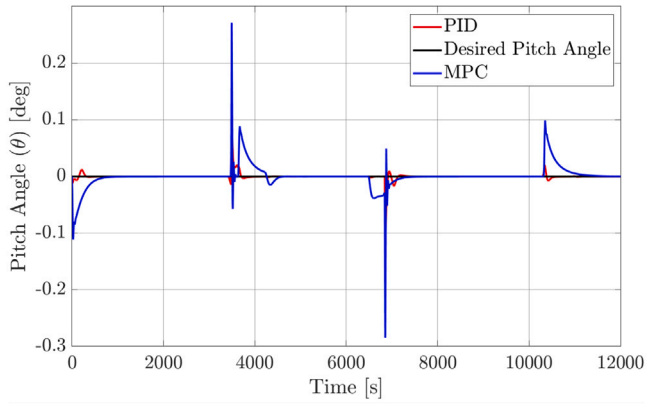

Fig. 12. PID and MPC pitch control comparison.

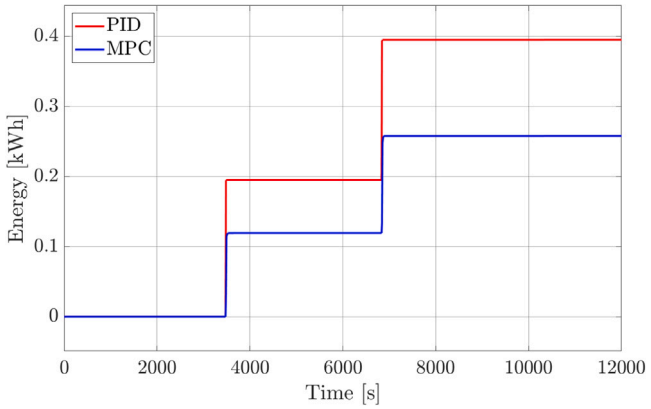

Fig. 15. PID and MPC TT energy consumption comparison.

of magnitude of the current deviation in Fig. 12 can still be considered negligible. The difference in control effort is shown in Fig. 14, where the peaks of the PID controller are higher compared to MPC, leading to the higher energy consumption shown in Fig. 15. Fine-tuning can be done for the pitch controller by slightly changing the weight factor in the weight matrices if it is preferred to decrease the maximum deviation of the pitch angle.

In Tables 7 and 8, the comparison between PID control and MPC can be found for depth and pitch control, respectively, based on some defined Key Performance Indicators (KPIs). Regarding the energy assessment, the maximum power and energy consumption are chosen as KPI. To assess the controller performance, the overshoot, settling time, and rise time are defined as KPI for the depth controller. For the pitch controller, only the maximum deviation in pitch angle is chosen as KPI,

Table 7
MPC and PID controllers depth control performance comparison over different KPIs (i.e., Maximum Power, Energy, Overshoot, Settling Time, Rise Time).

KPI	PID	MPC	Difference
Maximum power [kW]	46	47	+2%
Energy [kWh]	1.98	1.47	−26%
Overshoot [m]	0.879	0.0154	−98%
Settling time [s]	2129	620	−70%
Rise time [s]	200	286	+43%

Table 8
MPC and PID controllers pitch control performance comparison over different KPIs (i.e., Maximum Power, Energy, Overshoot).

KPI	PID	MPC	Difference
Maximum power [kW]	201	100	+50%
Energy [kWh]	0.40	0.26	−35%
Maximum deviation [deg]	0.12	0.27	+131%

Table 9
Overshoot analysis results.

PID	MPC
0.7935 ± 0.0025 [m]	0.0186 ± 0.0177 [m]

since the reference pitch angle is always zero degrees. From Figs. 7, 10, Tables 7, and 8, it can be seen that the rise time of MPC is somewhat slower compared to the PID controller. Furthermore, the MPC pitch controller's maximum deviation is larger than the PID controller, as already explained above. Besides these two KPIs, it can be concluded that overall the MPC outperforms the PID controller using the defined KPIs.

6.2. Sensitivity analysis

For the Monte Carlo simulation, 1000 simulations are done using PID control, and 1000 simulations are done using the MPC strategy, using randomly picked values from the six normally distributed coefficients described in Section 2. The results will be compared in this section, looking at the energy requirements for the tank systems and the controller performance.

In Fig. 16, the controller performance is assessed using the overshoot of the desired dredging depth of 15 m. It can be seen that the overshoot of the PID controller is located around the mean value of 0.7935 m, which can also be found in Table 9. In this table, the constructed 95% confidence intervals can also be found. To construct the 95% confidence intervals, the student's t-distribution is used, since for the random sample the standard deviation σ and mean μ are unknown parameters. When comparing the controller performance, it can be seen that the MPC depth controller has a larger range of both under- and overshoot, distributed around the mean value of 0.0403 m. The difference compared to the PID controller is the increased standard deviation, and corresponding larger confidence intervals. This indicates that the optimized solution of the MPC controller, taking into account the cost function and constraints, does not always prioritize close reference tracking. This results in the large range, taking into account the minimum and maximum values from the sample in Fig. 16. It must however be noted that the confidence interval of the mean value for the overshoot is still small, as can be seen in Table 9, and the overshoot within the 95% confidence interval is significantly smaller compared to the overshoot from the PID controller.

In Fig. 17, the results from the Monte Carlo simulation for the DCT energy requirements can be found. In Table 10, the corresponding 95% confidence intervals can be found. Both intervals are relatively small, and it can be seen that the sample mean of the DCT energy requirements is smaller using MPC, which corresponds to the previous conclusion that MPC is better at minimizing the energy requirements

Table 10
DCT energy requirements.

PID	MPC
1.9742 ± 0.0096 [kWh]	1.4082 ± 0.0067 [kWh]

Table 11
TT energy requirements.

PID	MPC
0.3960 ± 0.0027 [kWh]	0.2586 ± 0.0016 [kWh]

for depth control. In general, it can be said that uncertainties do not heavily affect the outcomes of the simulation model, considering the small confidence intervals. The confidence interval using MPC is smaller, from which it can be concluded that for depth control, MPC is better in handling uncertainties while minimizing the control effort and thus the corresponding energy requirements, compared to PID control.

In Fig. 18, the two normal distributions for the trim tank energy requirements are plotted, using MPC and PID control. The trim tanks are used to control the pitch angle, and the same conclusions can be drawn for the DCT used for controlling the depth. The 95% confidence intervals can be found in Table 11. MPC shows better performance in terms of control effort and corresponding energy requirements while having a smaller confidence interval compared to PID control. It can therefore also be concluded that MPC can better handle uncertainties in the state-space modeling approach, which leads to a smaller confidence interval. This conclusion corresponds to the conclusion for the depth controller.

7. Comparison with conventional dredging vessel

To support our proposed MPC framework and demonstrate the benefits of autonomous submerged dredging compared to conventional dredging, a comparison is made using a reference vessel. The ship used as a reference for the comparison and benchmarking is shown in Fig. 19.

To ensure a fair comparison, the energy requirements are calculated for the same operational profile, and a similar hopper volume is used. Previous research conducted as part of the Innovations in the Coastline Care program has calculated the required power for propulsion in transit, dredging, and discharging modes for both the conventional dredger and the ALERD, based on the defined operational profile and hopper volume.

The total energy consumption for the conventional dredger is found to be 3.75 kWh/m^3, while for the ALERD, the energy consumption is 1.09 kWh/m^3 without taking into account the energy requirements for stability and buoyancy control, which were unknown at the time of the research. The results of these calculations are presented in Tables 12 and 13. The comparison demonstrates that the ALERD consumes significantly less energy than the conventional dredger for the same operational profile and hopper volume, highlighting the potential advantages of autonomous submerged dredging. As a result of the present research, the energy requirements for stability and buoyancy control are estimated using the three tank systems, which need to be added to the energy requirements for the ALERD. The results of the calculations, and the corresponding total energy consumption, can be found in Table 12.

In Table 13, the final results of the comparison are reported. Using the same operational profile for both the conventional dredger and the ALERD, it can be seen that the energy consumption can be reduced by more than 66%.

A few important notes must be made regarding the assumptions made in this study. The MBT is utilized to compensate for changes in weight in the hopper to ensure weight balance. It is assumed that the mass flow rate of the MBTs and the hopper is equal and instantaneously available, only considering the constrained mass flow rate.

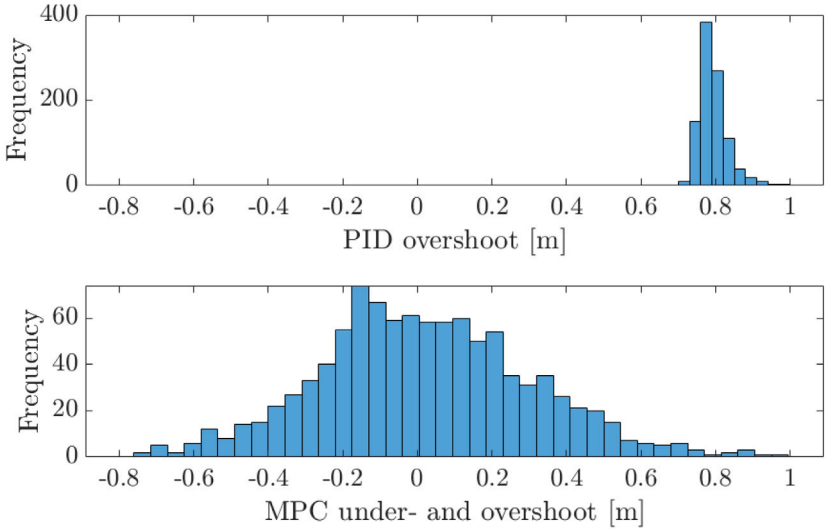

Fig. 16. Monte Carlo simulation results for controller performance.

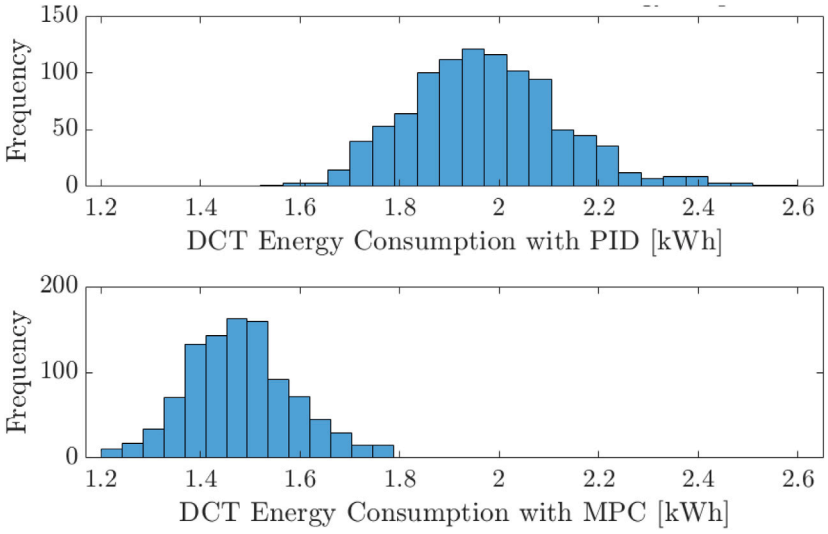

Fig. 17. Monte Carlo simulation results for DCT energy requirement.

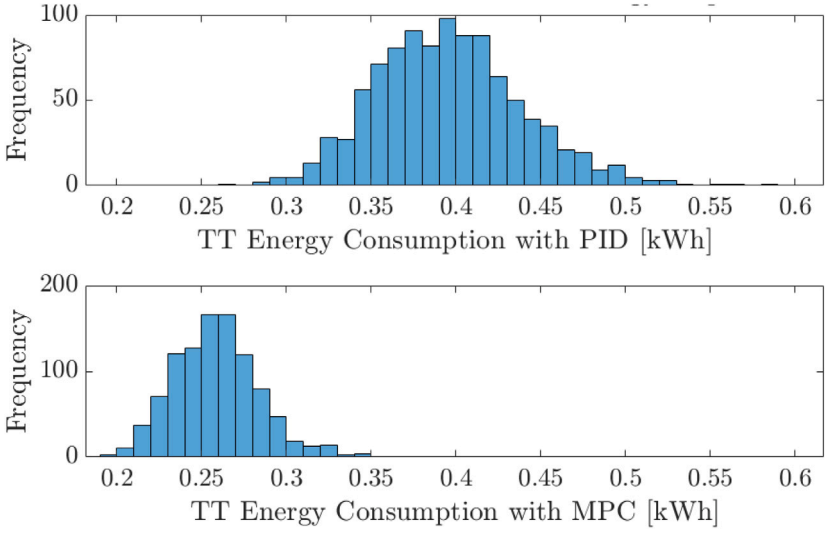

Fig. 18. Monte Carlo simulation results for TT energy requirement.

Fig. 19. Conventional dredger used as reference ship.

Table 12
ALERD energy consumption.

	Value	Unit
Hopper volume	2360	[m^3]
MBT energy consumption	408	[kWh]
DCT energy consumption	1.47	[kWh]
TT energy consumption	0.26	[kWh]
Energy consumption stability and buoyancy control	0.17	[kWh/m^3]
Energy consumption other systems	1.09	[kWh/m^3]
Total energy consumption	1.26	[kWh/m^3]

Table 13
Total energy requirements comparison.

Conventional dredger	ALERD	Difference
[kWh/m^3]		[%]
3.75	1.26	−66.4

The dynamics of the dredged soil and the free surface effect in the tanks and the hopper are not considered. Also, perfect loading and unloading conditions are assumed, meaning that the hopper is always symmetrically loaded and unloaded, leading to no additional trimming or rolling moments that need compensation. During the underwater operations of the ALERD, environmental disturbances are neglected. However, it is expected that disturbances such as waves, the near-bottom and surface effect, current, and changes in salinity and buoyancy require additional control effort, leading to an increase in energy requirements. It is important to note that the conclusion drawn in this study, that underwater dredging shows potential advantages compared to conventional dredging, is specific to the operational profile studied. The required energy for the pumps depends on the operating depth; hence, the potential advantages may vary with different operational profiles. Nevertheless, the calculations demonstrate promising results regarding the energy requirements for stability and buoyancy control, highlighting the potential advantages of submerged dredging.

8. Conclusions

This paper presents a model predictive control (MPC) strategy for an autonomous submerged dredging vehicle, with the aim of minimizing energy consumption during operation. To achieve this goal, a time-domain simulation model is developed using equations of motion in 6 degrees of freedom, which enables the manipulation of key input parameters, such as main dimensions or pump characteristics, to compare and optimize different designs. A benchmark proportional integral derivative (PID) controller is used for comparison, and the results demonstrate that the proposed MPC framework outperforms PID in terms of reference tracking of the desired depth and pitch angle, while minimizing the control effort. The simulation model is designed to enable the addition of the remaining degree of freedom, such as sway, roll, and yaw, to the controller, creating a complete 6-degree-of-freedom controlled simulation model. The impact of uncertainties in the input parameters is investigated, and the results show that MPC exhibits better performance in handling uncertainties, making it a more reliable tool. Moreover, the use of MPC reduces uncertainty in the simulation model's outcomes, enhancing its effectiveness. The results reveal that, for the specific operational profile defined in this paper, the vehicle controlled with MPC is more energy-efficient than the one controlled with PID control or a conventional dredger. Specifically, using the defined operational profile and a reference dredger with the same operational profile and similar hopper volume, the autonomous submerged dredging vehicle exhibits a lower energy consumption with a decrease of over 66%. Additionally, the contribution of the energy requirements for stability and buoyancy control to the total amount of consumed energy is only 13.5%, demonstrating the potential for submerged dredging as a sustainable and cost-effective solution for coastal replenishment along the Dutch coastline. In conclusion, this paper presents a robust and reliable MPC control strategy for an autonomous submerged dredging vehicle, providing excellent reference tracking performance while minimizing energy consumption. The simulation model is highly adaptable and can be used to compare different design parameters, demonstrating the potential of submerged dredging as a sustainable and cost-effective solution for coastal replenishment.

CRediT authorship contribution statement

Mathijs Bakker: Conceptualization, Methodology, Reviewing, Data curation, Writing – original draft, Software, Validation. **Andrea Coraddu:** Conceptualization, Methodology, Reviewing, Data curation, Writing – original draft, Writing – review & editing, Validation, Supervision. **Rolph Hijdra:** Conceptualization, Methodology, Reviewing, Supervision.

Declaration of competing interest

The authors declare that they have no known competing financial interests or personal relationships that could have appeared to influence the work reported in this paper.

Data availability

No data was used for the research described in the article.

References

Biegler, L., 2010. Nonlinear Programming: Concepts, Algorithms, and Applications To Chemical Processes. SIAM.

Boyd, S., Vandenberghe, L., 2004. Convex Optimization. Cambridge University Press.

Budiyono, A., 2011. Model predictive control for autonomous underwater vehicle. Indian J. Geo-Mar. Sci. 40, 191–199.

Carrica, P.M., Kim, Y., Martin, J.E., 2019. Near-surface self propulsion of a generic submarine in calm water and waves. Ocean Eng. 183, 87–105.

Elmokadem, T., Zribi, M., Youcef-Toumi, K., 2016. Trajectory tracking sliding mode control of underactuated AUVs. Nonlinear Dynam. 84 (2), 1079–1091.

Fletcher, R., 1981. Practical Methods of Optimization: Vol. 2: Constrained Optimization. John Wiley & Sons, Inc.

Fossen, T., 2011. Handbook of Marine Craft Hydrodynamics and Motion Control. Wiley, p. 596.

Fossen, T., Strand, J.P., 1999. Passive nonlinear observer design for ships using Lyapunov methods: full-scale experiments with a supply vessel. Automatica 35 (1), 3–16.

Gabriel, S.A., Cameron, A., Fowler, A., Pook, D.A., 2020. Modelling hydrodynamic loads for manoeuvring simulations of underwater vehicles. In: Proceedings of the 22nd Australasian Fluid Mechanics Conference AFMC2020. The University of Queensland.

Gao, T., Wang, Y., Pang, Y., Chen, Q., Tang, Y., 2018. A time-efficient CFD approach for hydrodynamic coefficient determination and model simplification of submarine. Ocean Eng. 154, 16–26.

Goldberg, D.E., 1989. Genetic Algorithms in Search, Optimization and Machine Learning. Addison-wesley.

Guo, L., Gao, B., Li, Y., Chen, H., 2017. A fast algorithm for nonlinear model predictive control applied to hev energy management systems. Sci. China Inf. Sci. 60, 1–17.

Hammad, M.M., Elshenawy, A.K., El Singaby, M.I., 2017. Trajectory following and stabilization control of fully actuated auv using inverse kinematics and self-tuning fuzzy PID. PLoS One 12 (7).

Healey, A.J., Lienard, D., 1993. Multivariable sliding-mode control for autonomous diving and steering of unmanned underwater vehicles. IEEE J. Ocean. Eng. 18 (3), 327–339.

Hijdra, R., Van Der Harst, S., 2019. Design of an autonomous underwater maintenance dredger: A teaser to the maritime industry. In: Journal of Physics: Conference Series. vol. 1357, IOP Publishing, p. 12001.

Imlay, F., 1961. The complete expressions for added mass of a rigid body moving in an ideal fluid. p. 31, URL http://oai.dtic.mil/oai/oai?verb=getRecord&metadataPrefix=html&identifier=AD0263966.

Jalving, B., 1994. The NDRE-AUV flight control system. IEEE J. Ocean. Eng. 19 (4), 497–501.

Jordán, M.A., Bustamante, J.L., 2009. Adaptive Control for Guidance of Underwater Vehicles. pp. 251–278.

Karimi, H.R., Lu, Y., 2021. Guidance and control methodologies for marine vehicles: A survey. Control Eng. Pract. 111, 104785.

Kerrigan, E., Maciejowski, J., 2002. Designing model predictive controllers with prioritised constraints and objectives. In: Proceedings. IEEE International Symposium on Computer Aided Control System Design. IEEE, pp. 33–38.

Kong, F., Guo, Y., Lyu, W., 2020. Dynamics modeling and motion control of an new unmanned underwater vehicle. IEEE Access 8, 30119–30126.

Lee, S.K., Joung, T.H., Cheon, S.J., Jang, T.S., Lee, J.H., 2011. Evaluation of the added mass for a spheroid-type unmanned underwater vehicle. Int. J. Naval Archit. Ocean Eng. 3 (3), 174–180.

Londhe, P.S., Dhadekar, D.D., Patre, B.M., Waghmare, L.M., 2017. Uncertainty and disturbance estimator based sliding mode control of an autonomous underwater vehicle. Int. J. Dyn. Control 5 (4), 1122–1138.

Londhe, P.S., Patre, B.M., 2019. Adaptive fuzzy sliding mode control for robust trajectory tracking control of an autonomous underwater vehicle. Intell. Serv. Robot. 12 (1), 87–102.

Long, C., Qin, X., Bian, Y., Hu, M., 2021. Trajectory tracking control of ROVs considering external disturbances and measurement noises using ESKF-based MPC. Ocean Eng. 241, 109991.

Ma, Y., Sui, D., Xing, Y., Ong, M.C., Hemmingsen, T.H., 2021. Depth control modelling and analysis of a subsea shuttle tanker. In: Proceedings of the International Conference on Offshore Mechanics and Arctic Engineering - OMAE. vol. 5.

Mayne, D.Q., Rawlings, J.B., Rao, C.V., Scokaert, P.O., 2000. Constrained model predictive control: Stability and optimality. Automatica 36 (6), 789–814.

Nocedal, J., Wright, S.J., 1999. Numerical Optimization. Springer.

Prestero, T., 2001. Development of a six-degree of freedom simulation model for the remUS autonomous underwater vehicle. In: MTS/IEEE Oceans 2001. an Ocean Odyssey. Conference Proceedings. vol. 1, pp. 450–455 vol.1.

Rawlings, J.B., Mayne, D.Q., 2009. Model Predictive Control: Theory and Design. vol. 825, Nob Hill Publishing.

Renilson, M., 2015. Submarine Hydrodynamic. Springer Briefs in Applied Sciences and Technology.

Rout, R., Subudhi, B., 2017. Inverse optimal self-tuning PID control design for an autonomous underwater vehicle. Internat. J. Systems Sci. 48 (2), 367–375.

Sahoo, A., Dwivedy, S.K., Robi, P.S., 2019. Advancements in the field of autonomous underwater vehicle. Ocean Eng. 181, 145–160.

Severholt, J., 2017. Generic 6-DOF added mass formulation for arbitrary underwater vehicles based on existing semi-empirical methods. p. 51, URL http://www.diva-portal.org/smash/get/diva2:1127931/FULLTEXT01.pdf.

Steenson, L.L.V., Phillips, A.A.B., Rogers, E., Furlong, M.E., Turnock, S.R., 2011. Control of an AUV from thruster actuated hover to control surface actuated flight. pp. 1–13, URL http://leo-steenson.com/Documents/RTO-MP-AVT-189-Steenson2011.pdf.

Steenson, L.V., Turnock, S.R., Phillips, A.B., Harris, C., Furlong, M.E., Rogers, E., Wang, L., Bodles, K., Evans, D.W., 2014. Model predictive control of a hybrid autonomous underwater vehicle with experimental verification. Proc. Inst. Mech. Eng. M: J. Eng. Mar. Environ. 228 (2), 166–179.

Takahashi, K., Sahoo, P.K., 2020. Numerical study on the hydrodynamic performance of the darpa suboff submarine for steady translation. In: Proceedings of the International Conference on Offshore Mechanics and Arctic Engineering - OMAE. vol. 8, American Society of Mechanical Engineers (ASME).

Tanakitkorn, K., Wilson, P.A., Turnock, S.R., Phillips, A.B., 2017. Depth control for an over-actuated, hover-capable autonomous underwater vehicle with experimental verification. Mechatronics 41.

Tang, L., Yan, F., Zou, B., Wang, K., Lv, C., 2020. An improved kinematic model predictive control for high-speed path tracking of autonomous vehicles. IEEE Access 8, 51400–51413.

Tian, Y., Yao, Q., Hang, P., Wang, S., 2022. Adaptive coordinated path tracking control strategy for autonomous vehicles with direct yaw moment control. Chin. J. Mech. Eng. 35 (1), 1–15.

Tijjani, A.S., Chemori, A., Creuze, V., 2021. Robust adaptive tracking control of underwater vehicles: Design, stability analysis, and experiments. IEEE/ASME Trans. Mechatronics 26 (2), 897–907.

Valeriano-Medina, Y., Martinez, A., Hernandez, L., Sahli, H., Rodriguez, Y., Cañizares, J.R., 2013. Dynamic model for an autonomous underwater vehicle based on experimental data. Math. Comput. Model. Dyn. Syst. 19 (2), 175–200.

von Ellenrieder, K.D., 2021. Control of Marine Vehicles. Springer.

Xiang, X., Yu, C., Zhang, Q., 2017. Robust fuzzy 3D path following for autonomous underwater vehicle subject to uncertainties. Comput. Oper. Res. 84, 165–177.

Xu, Y., Tang, W., Chen, B., Qiu, L., Yang, R., 2021. A model predictive control with preview-follower theory algorithm for trajectory tracking control in autonomous vehicles. Symmetry 13 (3), 381.

Yan, Z., Gong, P., Zhang, W., Wu, W., 2020. Model predictive control of autonomous underwater vehicles for trajectory tracking with external disturbances. Ocean Eng. 217.

Yildiz, O., Gökalp, R.B., Yilmaz, A.E., 2009. A review on motion control of the underwater vehicles. In: 6th International Conference on Electrical and Electronics Engineering. IEEE.

Yu, S., Hirche, M., Huang, Y., Chen, H., Allgöwer, F., 2021. Model predictive control for autonomous ground vehicles: A review. Autonom. Intell. Syst. 1, 1–17.

Zhang, Y., Liu, X., Luo, M., Yang, C., 2019. MPC-based 3-D trajectory tracking for an autonomous underwater vehicle with constraints in complex ocean environments. Ocean Eng. 189, 106309.